

## Numerical Simulation for Cylindrical Electrostatic Precipitator: Effect of the Applied Voltage

Athraa A. Hussein<sup>1a\*</sup> and Thamir H. Khalaf<sup>1b</sup>

<sup>1</sup>Department of physics, College of Science, University of Baghdad, Baghdad, Iraq

<sup>b</sup>E-mail: drthamirhameed@gmail.com

<sup>a\*</sup>Corresponding author: athraa.hussein1204@sc.uobaghdad.edu.iq

### Abstract

Coaxial (wire-cylinder) electrodes arrangements are widely used for electrostatic deposition of dust particles in flue gases, when a high voltage is applied to electrodes immersed in air and provide a strongly non-uniform electric field. The efficiency of electrostatic filters mainly depends on the value of the applied voltage and the distribution of the electric field. In this work, a two-dimensional computer simulation was constructed to study the effect of different applied voltages (20, 22, 25, 26, 28, 30 kV) on the inner electrode and their effect on the efficiency of the electrostatic precipitator. Finite Element Method (FEM) and COMSOL Multiphysics software were used to simulate the cross section of a wire cylinder. The results showed that the velocity of the liquid and the charge accumulation of the particles increased with the increase of the applied voltage and also the efficiency of the precipitator increased and reached 100% with an applied voltage of 30 kV.

### Article Info.

#### Keywords:

*Electrostatic precipitator, Simulation, COMSOL Multiphysics, Finite element method, DC Corona discharge.*

#### Article history:

*Received: Jul. 07,2022*

*Accepted: Aug.22,2022*

*Published: Dec.01,2022*

### 1. Introduction

Nowadays, global warming is the biggest challenge for all human beings in the world due to the huge increase in emissions especially from heavy industry plants such as coal-fired power plants, bio-energy plants, waste plants, cement kilns, glass kilns, biomass energy and atomization Thermal coal, and other consumption patterns, in the energy industry have been identified as the main sources of particulate emissions. Consequently, treatment is a significant issue to reduce or total eliminate the emissions by using the electrostatic precipitators (ESP) to reduce the pollutions from the heavy factories [1-6]. The electrostatic precipitator is a widely used device for removing particles from a gas stream, using an induced electrostatic charge [7].

When gas molecules and dust particles flow across wires with high DC voltage, the gas molecules are ionized, creating a phenomenon known as "corona discharge". When particles are charged, they are drawn to collecting plates, which are plates with opposing charges. Wen and Su [8] investigated the distinctive changes of the cylindrical corona electrodes utilized in an ESP during prolonged operation, as well as changes in the diameter and pitch of the electrodes. Their findings showed that the characteristics were most significantly influenced by the electric field surrounding the cylindrical corona electrodes. When the electric field surrounding the cylindrical corona electrodes is strong, the collection efficiency is high and the oxidation is severe. Krachai et al. [9] experimentally studied a new geometry of the electrostatic precipitator in corona discharge DC for both positive and negative electrodes. The designed electrostatic precipitator includes an iron wire electrode of 0.25 mm in diameter and 520 mm in length and five grounded cylindrical electrodes using incense particles as a test sample. 100% collection efficiency was achieved with relatively low power consumption of 1.5 W at an applied voltage of 9 kV. The main advantage of electrostatic precipitator's is that they have no significant pressure drop and collection

efficiency can be 99.5 % or more. In this work, the effect of different voltages on the efficiency of the electrostatic precipitator was studied.

## 2. Modeling of the Problem

### 2.1. Governing Equations

The engineering of a coaxial electrode (wire cylinder) was used to model the electrostatic precipitator. In this model, the Poisson's equation and the charge conservation equation are coupled to compute the movement of a charge carrier. Drift in the electric field and convection are both involved in charge carrier movement. Without source terms the domain equations are [10]:

$$\nabla \cdot J = 0 \quad (1)$$

$$J = z_q \mu \rho_q E + \rho u \quad (2)$$

$$\varepsilon_0 \nabla^2 V = -\rho_q \quad (3)$$

where:  $J$  is the current density,  $z_q$  is the charge number,  $\mu$  is the mobility,  $\rho_q$  is the space charge number density,  $E$  is the electric field,  $u$  is the fluid velocity,  $V$  is electric potential, and  $\varepsilon_0$  is the vacuum permittivity. The transport equation given by manipulating this set of equations as below:

$$\mu \left( \frac{\rho_q^2}{\varepsilon_0} - \nabla V \cdot \nabla \rho_q \right) + \nabla \rho_q \cdot u = 0 \quad (4)$$

where it is assumed that the mobility is constant. It is interesting to note that the domain equations do not contain any information related to plasma creation and maintenance. All plasma physics is condensed in the boundary conditions for the inner electrode.

### 2.2. Laminar Flow Model

The laminar flow interface is used to solve for the fluid velocity and pressure [11]:

$$\begin{aligned} \rho(u \cdot \nabla)u &= \nabla \cdot [-p I + \mu (\nabla u + (\nabla u)^T)] + F_{EHD} \\ \nabla \cdot u &= 0 \end{aligned} \quad (5)$$

where:  $\mu$  is the dynamic viscosity,  $\rho$  is the fluid density,  $p$  is the pressure, and  $F_{EHD}$  is the electrohydrodynamic force define as:

$$F_{EHD} = \rho_q \quad (6)$$

### 2.3. Particle Tracing Model

Following Newton's second law, the particle locations are calculated by solving second-order equations of motion for the vector elements that make up the particle position:

$$\begin{aligned} \frac{dq}{dt} &= v \\ \frac{d}{dt}(m_p v) &= F_t \end{aligned} \quad (7)$$

where:  $q$  is the particle position,  $v$  is the particle velocity,  $m_p$  is the particle mass, and  $F_t$  is the total force. The forces acting on the particles are the drag force and the electric force. Rarefaction effects need to be included in the drag force because the particle radii become very small. The drag force  $F_D$  is described with the Cunningham-Millikan-Davis model:

$$F_D = \frac{1}{\tau_p s} \tag{8}$$

$$\tau_p = \frac{4\rho_p d_p^2}{3\mu C_D Re_r} \tag{9}$$

where:  $\tau_p$  is the particle velocity response time,  $\rho_p$  is the density of the particle,  $d_p^2$  is the particle diameter,  $C_D$  is the drag coefficient, and  $Re_r$  is the relative Reynolds number given by the expression:

$$Re_r = \frac{\rho \|u-v\| d_p}{\mu} \tag{10}$$

and  $S$  is the drag correction coefficient defined as:

$$S = 1 + Kn \left( C_1 + C_2 \exp\left(-\frac{C_3}{Kn}\right) \right) \tag{11}$$

The electric force  $F_e$  acting on the particles is defined as:

$$F_e = eZE \tag{12}$$

where:  $e$  is the elementary charge and  $Z$  is the accumulated charge number on each particle. The charge accumulated on the particles is computed with the Lawless model:

$$\tau_c \frac{dz}{dt} = \begin{cases} R_f + f_a & (|v_e| \leq |v_s|) \\ R_d f_a & (|v_e| > |v_s|) \end{cases} \tag{13}$$

where  $\tau_c$  is the characteristic charging Time

$$\tau_c = \frac{e^2}{4\pi\rho_q\mu K_B T_i} \tag{14}$$

where:  $K_B$  is Boltzmann constant and  $T_i$  is the ion temperature.  $R_f$  and  $R_d$  are the dimensionless charging rates due to field and diffusion transport, respectively, defined as:

$$R_f = \frac{v_s}{4\epsilon_0} \left(1 - \frac{v_e}{v_s}\right)^2 \tag{15}$$

$$R_d = \frac{v_e - v_s}{\exp(v_e - v_s) - 1} \tag{16}$$

where

$$v_e = \frac{Ze^2}{4\pi\epsilon_0 r_p K_B T_i} \tag{17}$$

$$v_s = 3\omega_e \frac{\epsilon_{r,p}}{\epsilon_{r,p} + 2} \tag{18}$$

$$\omega_e = \frac{er_p|E|}{K_B T_i} \tag{19}$$

where:  $\varepsilon_{r,p}$  is the relative permittivity of the particles.  $f_a$  is a function used to join the diffusion and field charging rates defines as [10]:

$$f_a = \begin{cases} \frac{1}{(\omega_e + 0.475)^{0.575}} & (\omega_e \geq 0.525) \\ 1 & (\omega_e < 0.525) \end{cases} \quad (20)$$

#### 2.4. Boundary Condition

The boundary condition for Poisson's equation is the normal component of the electric field at the corona electrode.

$$\mathbf{n} \cdot \mathbf{E} = E_0 \quad (21)$$

Zero charge at the inlet and outlet as well as  $V = 0$  at the collection plates serve as additional boundary conditions for Poisson's equation. Eq. (4) boundary condition requires employing a Lagrange multiplier to get the space charge density  $\rho_q$  at the corona electrode in order to confirm the imposed potential  $V_0$ .

$$V - V_0 = 0 \quad (22)$$

At the corona electrode, both potential and electric field are imposed in this model. The value of the electric field at the wire must be sufficiently near the actual one in order to produce physically predicative results. Here, Peek's law is applied [12]:

$$E_0 = 3 \times 10^6 \sigma \left( 1 + \frac{0.03}{\sqrt{\sigma r_i}} \right) \quad (23)$$

where:  $E_0$  is the breakdown electric field,  $\sigma$  is the gas number density normalized to the gas density at 760 torr and 293.15 K, and  $r_i$  is the radius of the corona electrode.

### 3. Geometry and Mesh

This work is an electrostatic precipitator simulation through a two-dimensional system of a coaxial geometric electrode (wire cylinder) as shown in Fig. 1. It is possible to solve the model in two-dimensional axial symmetry to reduce the execution time, but in this work the simulation was done in two dimensions to know the results in all parts of the precipitator and because the simulation in two dimensions is closer to practical experiments. To perform the simulation in this model, a cross section of the wire cylinder was considered as shown in Fig.2. The DC high voltage source was located on the inner electrode and the cylinder was grounded. The finite element method was used to solve the proposed model, in which the solution area was divided into small elements, and the elements of the distribution network were applicable to all areas. The majority of the most significant events occurred at the boundary, so it was necessary to achieve greater network resolution in these regions as shown in Fig.3. The plasma was generated near the inner electrode and the density of ions was high as a result of ionization, but in the region between the electrodes near the cylinder, a charging process occurred and particles precipitated. The configuration consisted of a small radius of 0.0005 m wire representing the corona wire and a grounded cylinder with a radius of 0.1 m and a length of 0.7 m. The left side represents the entrance and the right side represents the exit. A high voltage DC

source of different values (20, 22, 25, 26, 28, 30 kV) was applied to the inner electrode to study its effect on the efficiency of the precipitator. As the particles were released from the inlet on the left, they were transported within the liquid. The particles accumulate charge along their paths and are subjected to electric forces that deflect their paths in the direction of the collecting cylinder. The operating conditions of the electrostatic precipitator are shown in Table 1, while the input parameters of the model are shown in Table 2.

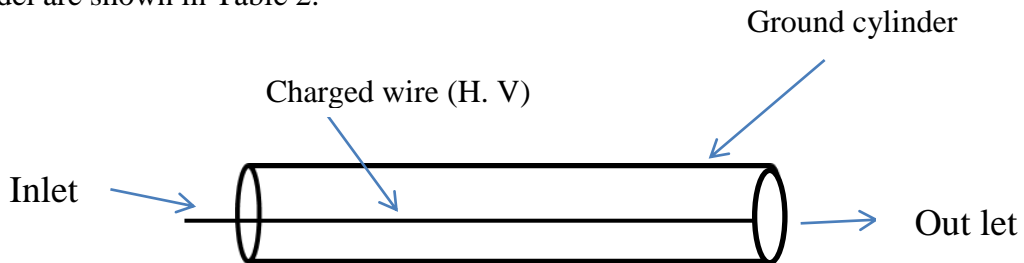


*Figure 1: Schematic diagram of the Wire-cylinder electrodes geometry.*

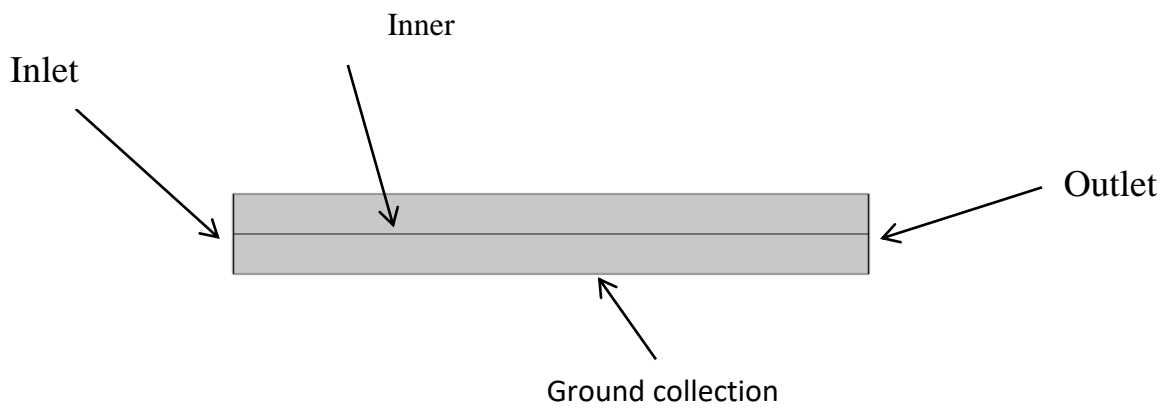


*Figure 2: Cross section for a (wire-cylinder).*

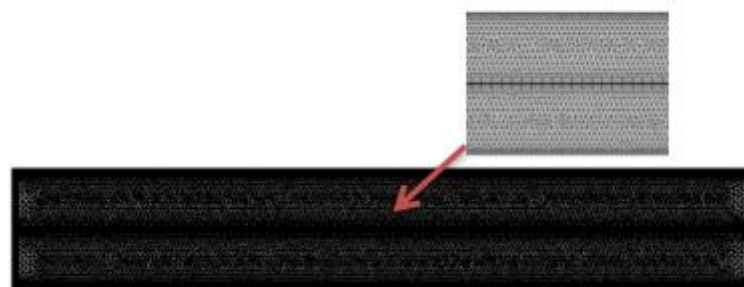


*Figure 3: The finite element distribution in 2D.*

**Table 1: Operation conditions of the electrostatic precipitator.**

Temperature	293.15 K
Pressure	1 atm
Average Inlet fluid velocity	1 m/s

**Table 2: Input parameters of model.**

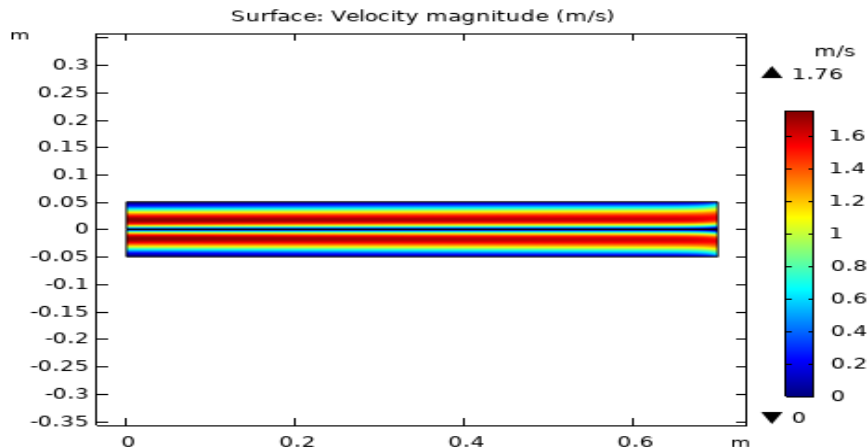
Inner electrode radius	0.0005 m
length of cylinder	0.7 m
radius of cylinder	0.1 m
Reduced ion mobility	$3 \times 10^{21} [1/(V.m.s)]$
Initial Value of space charge density	$1.0 \times 10^{-5} [C/m^3]$

#### 4. Results and Discussion

The electrostatic precipitator was simulated by a two-dimensional system of a coaxial geometric electrode (wire-cylinder). Different voltage values of (20, 22, 25, 26, 28, 30 kV) were applied to the inner electrode to find out their effect on the efficiency of the precipitator. This simulation was conducted using COMSOL 5.6.

##### 4.1. Fluid Velocity

The fluid velocity is an important parameter of the electrostatic precipitator. The model results showed that the fluid velocity was practically not affected by the electrohydrodynamic force, and the drift velocity was always much greater than the fluid velocity in the regions of interest. The fluid velocity was obtained by solving Eqs. (5) and (6). Fig.4 shows the distribution of fluid velocity along the length of the cylinder in the direction of stretching the cylinder (z-axis) with an applied voltage of 26 kV, where the x-axis represents the length of the cylinder and the y-axis represents the height of the cylinder. It is noted from the figure that near the inner electrode (cathode electrode), the velocity distribution values are low and gradually increase outward towards the other electrode (grounded cylinder), as indicated by the color gradient.

**Figure 4: Velocity magnitude of the flow in the electrostatic precipitator.**

## 4.2. Electric Potential

The electric potential is an important parameter of the electrostatic precipitator, as it is the main parameter on which the electric field depends. In this model, both the potential and the electric field were imposed on the internal electrode, where the potential and electric field were calculated using Eqs. (21), (22), and (23). Fig.5 represents the electric potential distribution inside the cylinder at an applied voltage of 26 kV, where the x-axis represents the length of the cylinder and the y-axis represents the height of the cylinder. From the figure, it can be seen that the electric potential distribution values increased near the inner electrode and gradually decreased outward towards the other electrode (grounded cylinder) as shown in the color gradation.

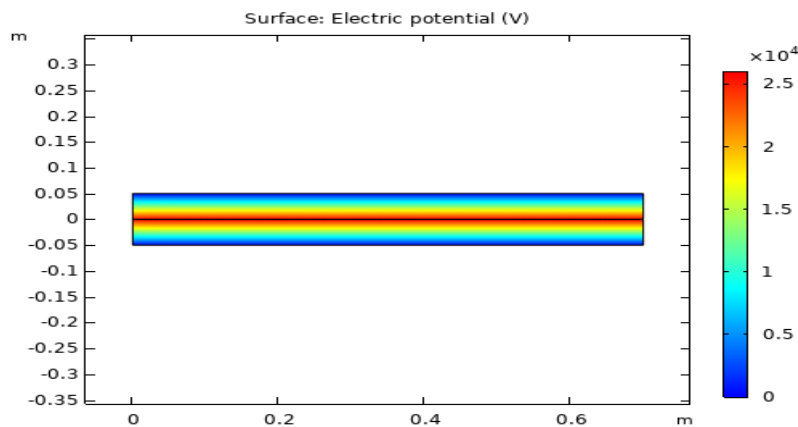


Figure 5: Electric potential distribution.

## 4.3. Accumulated Charge Number

Fig.6 shows the number of charges accumulated on the particles inside the cylinder at applied voltage of 26 kV where the x-axis represents the radius of the particles and the y-axis represents the accumulated charge number. The charge accumulated on the particles was calculated using the Lawless model from Eqs. (13) to (20). It can be seen that the radius of the particles plays an important role in the process of charge accumulation on particles as the charge accumulation increases on particles with large radii compared to particles with low radii.

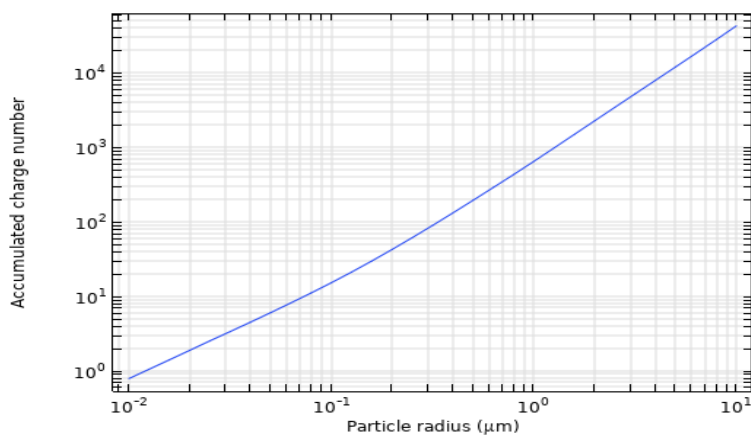
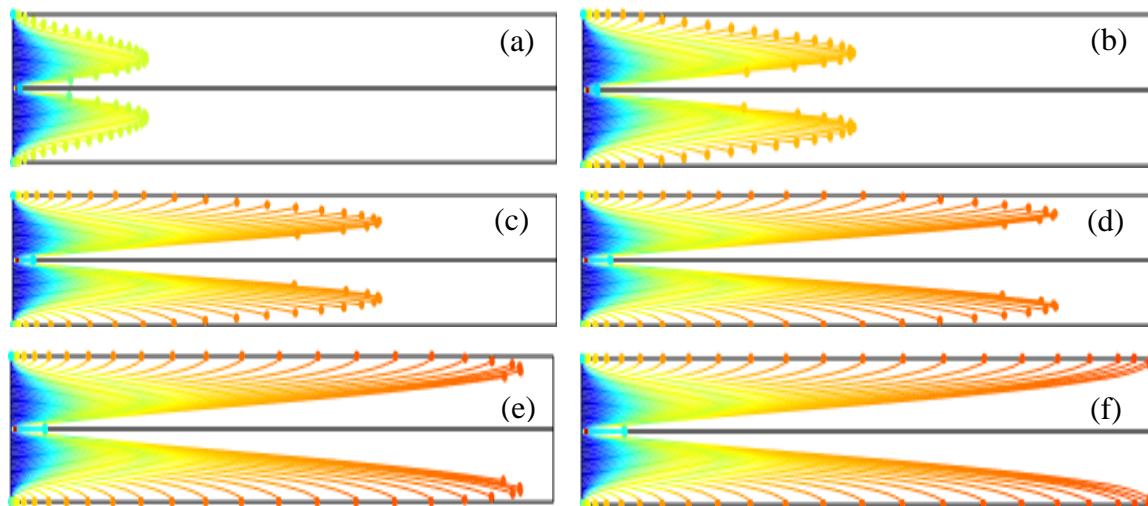


Figure 6: Average charge accumulated per particle at the last time step as function of particle radius.

## 5. The Time Development of the Particle Trajectory

Fig.7 shows the particle trajectory with an applied voltage of 26 kV as the particles were released from the left inlet and were gradually transported in the fluid flow towards the right outlet. Where the x-axis represents the length of the cylinder and the y- axis represents the height of the cylinder. From Fig.7, the gradual trajectory of the particles at different times can be noted, where the particles were close to the entrance with a time of 0.1 seconds and reached the middle in a time of 0.3 seconds and gradually moved until they reached the exit on the right side at a time of 0.6 seconds.



*Figure 7: Time development of the particle trajectory for particles with a radius of 0.2  $\mu\text{m}$  at different time a) 0.1s b) 0.2s, c) 0.3s, d)0.4s, e)0.5s, f)0.6s.*

## 6. The Effect of the Applied Voltage of Efficiency Electrostatic Precipitator

Different voltages applied to the inner electrode positively affected the efficiency of the electrostatic precipitator, as higher voltages enhanced the charge of the particles, and the particles gradually became charged along their path resulting in electric forces that deflected their path towards the wall. The particle radius affects the balance of drag and the electric force felt by the particles, which affects the particle trajectory and the assembly efficiency of the electrostatic precipitator. Fig.8 shows the particle collection efficiency and the average particle charge in the last time step as a function of the particle's radii of different sizes (0.01-10  $\mu\text{m}$ ) and the different voltages applied to the inner electrode. Particle size plays an important role in how a particle is charged because the diffusion charge mechanism is the most prevalent factor on small particles, while field charge is more diffuse on larger particles; larger particles get more electric charge, smaller particles get less electric charge because they are subjected to less drag; at a different voltage applied to the inner electrode, the collection efficiency is greater at maximum particle dimensions. Larger particles were collected more efficiently because they gained more electric charge, while smaller particles were collected more efficiently because they were subjected to less drag. It can be seen that the particle collecting efficiency increased with the increase in

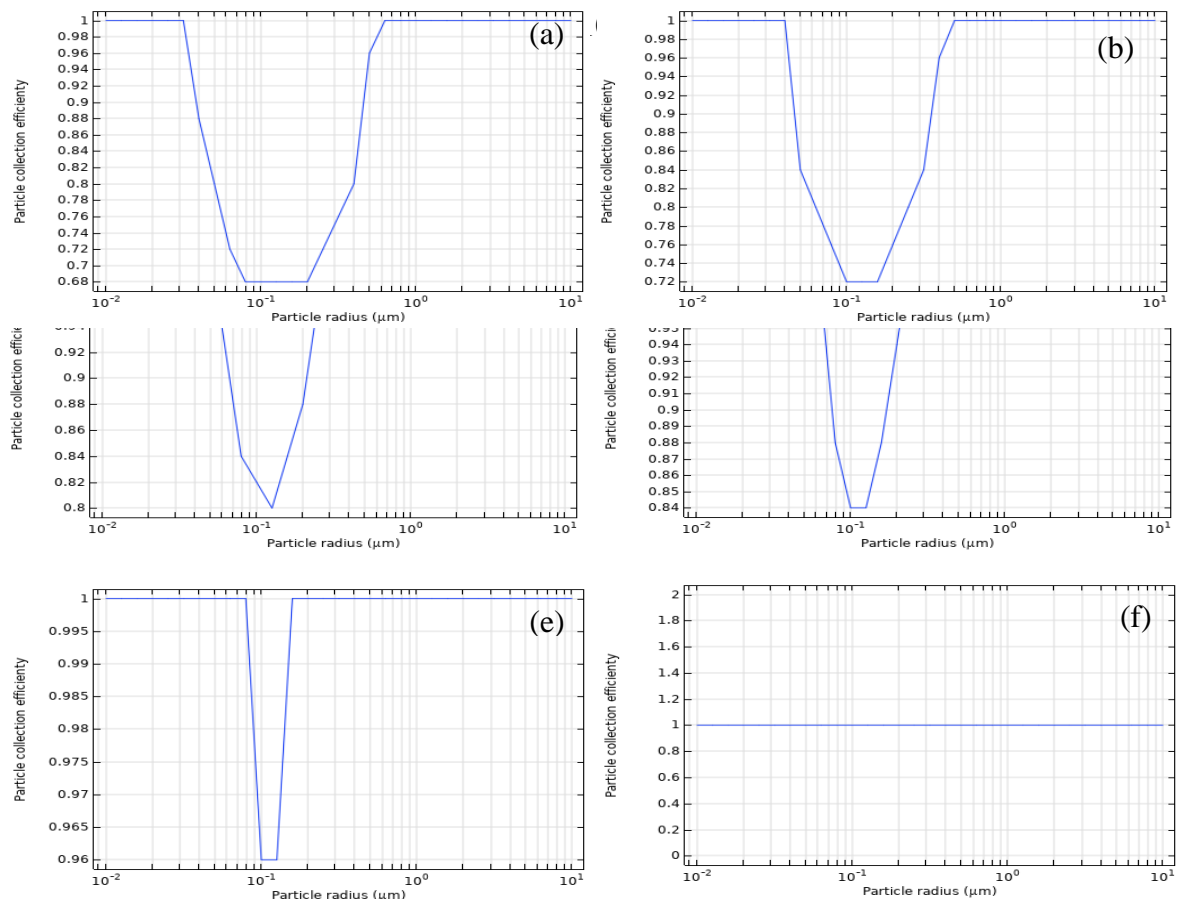


**Figure 8: Particle collection efficiency as a function of the particle radius for different applied voltage a) 20kv, b) 22kv, c) 25kv, d) 26kv, e) 28kv, f) 30kv.**

## 7. Conclusions

In this paper, a two-dimensional computer simulation was implemented using COMSOL Multiphysics 5.6 program to study the effect of different applied voltages (20,22, 25, 26, 28, 30 kV) between the electrodes on the efficiency of the electrostatic precipitator. The inner electrode had a radius of 0.0005 m, a width of 0.7 m, a cylinder radius of 0.1 m, width of 0.7 m, and a flow rate of 1 m/s. The results showed that the fluid velocity and charge accumulation increased with the increase in the applied voltage, as well as an increase in the efficiency of the precipitator, and the efficiency of 100% was reached with an applied voltage of 30 kV.

## Acknowledgements

The authors would like to thanks the Department of Physics, College of Science, University of Baghdad.

## Conflict of interest

Authors declare that they have no conflict of interest.

## References

1. Martínez T. J., Pastor P. J., Sancho Val J., McNabola A., Martínez C. M., and Gallagher J., *A Functional data analysis approach for the detection of air*

- pollution episodes and outliers: a case study in Dublin, Ireland. Mathematics*, 2020. **8**(2): pp. 225(1-20).
2. Zheng C., Liu X., Yan P., Zhang Y., Wang Y., Qiu K., and Gao X., *Measurement and prediction of fly ash resistivity over a wide range of temperature. Fuel*, 2018. **216**: pp. 673-680.
  3. Li D. and Cheng Y., *Evaluation of gas control ability of a coal and gas outburst mine. Energy Sources, Part A: Recovery, Utilization, Environmental Effects*, 2014. **36**(21): pp. 2401-2409.
  4. Hu J., Lei T., Wang Z., Yan X., Shi X., Li Z., He X., and Zhang Q., *Economic, environmental and social assessment of briquette fuel from agricultural residues in China—a study on flat die briquetting using corn stalk. Energy*, 2014. **64**: pp. 557-566.
  5. Yang Z., Zheng C., Li Q., Zheng H., Zhao H., and Gao X., *Fast evolution of sulfuric acid aerosol activated by external fields for enhanced emission control. Environmental Science Technology*, 2020. **54**(5): pp. 3022-3031.
  6. Zheng C., Zheng H., Shen J., Gao W., Yang Z., Zhao Z., Wang Y., Zhang H., and Gao X., *Evolution of condensable fine particle size distribution in simulated flue gas by external regulation for growth enhancement. Environmental Science Technology*, 2020. **54**(7): pp. 3840-3848.
  7. Dong M., Zhou F., Zhang Y., Shang Y., and Li S., *Numerical study on fine-particle charging and transport behaviour in electrostatic precipitators. Powder Technology*, 2018. **330**: pp. 210-218.
  8. Wen T.-Y. and Su J.-L., *Corona discharge characteristics of cylindrical electrodes in a two-stage electrostatic precipitator. Heliyon*, 2020. **6**(2): pp.1-6.
  9. Berkane Krachai C., *Experimental modelling of wire-to-multicylinder electrostatic precipitator. Przegląd Elektrotechniczny*, 2020. **96**(10): pp.179-183.
  10. Zheng C., Zhang X., Yang Z., Liang C., Guo Y., Wang Y., and Gao X., *Numerical simulation of corona discharge and particle transport behavior with the particle space charge effect. Journal of Aerosol Science*, 2018. **118**: pp. 22-33.
  11. Wang J.J., Malissa J.D., Phillips III J.R., Johansen M.R., Calle C.I., and Buhler C.R. *Numerical model of the mars electrostatic precipitator. in COMSOL Conference*. 2019.
  12. Potrymai E. and Perstnov I., *Time dependent modelling and simulation of the corona discharge in electrostatic precipitators, Master Thesis, Linnaeus University*, 2014.

## محاكاة عددية للمررب الكهروستاتيكي الأسطواني: تأثير الجهد المطبق

عذراء علي حسين<sup>1</sup> وثامر حميد خلف<sup>1</sup>

<sup>1</sup> قسم الفيزياء، كلية العلوم، جامعة بغداد، بغداد، العراق

### الخلاصة

تستخدم ترتيبات قطب السلك المحوري (wire-cylinder) على نطاق واسع للترسيب الكهروستاتيكي لجزيئات الغبار الموجودة في غازات المداخن، عندما يتم تطبيق جهد عال على الأقطاب الكهربائية المغمورة في الهواء وتوفر مجالاً كهربائياً غير منظم بقوة. تعتمد كفاءة المرشحات الكهروستاتيكية بشكل أساسي على قيمة الجهد المطبق وتوزيع المجال الكهربائي. ان اساس عمل المررب الكهروستاتيكي هو تفريغ الاكليل الموجب المستمر. في هذا العمل تم عمل محاكاة حاسوبية ثنائية الأبعاد (2D) لدراسة تأثير الفولتية التطبيقية المختلفة (30 kV , 28 , 26 , 25 , 22 , 20) على القطب الداخلي وتأثيرها على كفاءة المررب الكهروستاتيكي. تم استخدام طريقة العناصر المحدودة (FEM) وبرنامج COMSOL Multiphysics لإجراء المحاكاة على المقطع العرضي للأسطوانة السلكية. أظهرت النتائج أن سرعة السائل وتراكم الشحنة للجسيمات تزداد مع زيادة الجهد المطبق كما لوحظ تحسين في زيادة كفاءة المررب الكهروستاتيكي مع زيادة الفولتية المطبقة على القطب الداخلي حيث تم الوصول إلى كفاءة 100% عند جهد مطبق (30) كيلو فولت.